Journal of Experimental Marine Biology and Ecology 503 (2018) 136–146

Contents lists available at ScienceDirect

Journal of Experimental Marine Biology and Ecology

journal homepage: www.elsevier.com/locate/jembe

A simple, user friendly tool to readjust raw PAM data from field measurements to avoid over- or underestimating of microphytobenthos photosynthetic parameters

Jérôme Morelle[1], Francis Orvain*,[1], Pascal Claquin

Normandie Université, Université de Caen Normandie, UMR BOREA, CNRS-7208, IRD-207, MNHN, UPMC, UCBN, Esplanade de la paix, F-14032 Caen, France

ARTICLE INFO

Keywords:
Chlorophyll *a*
Depth distribution
Light attenuation coefficient
Microphytobenthos
Sediment
PAM
Primary productivity

ABSTRACT

Intertidal mudflats are among the most productive ecosystems and microphytobenthic (MPB) biofilms play a key role in primary production. MPB primary production varies at short spatial and temporal scales. Accurate measurements thus require rapid non-intrusive methods like pulse amplitude modulate (PAM) fluorescence. However, the effect of granulometry and chl *a* concentration profile in light attenuation on irradiance and on fluorescence signal in the photic layer need to be taken into account when primary production is estimated using PAM. We propose a tool to readjust raw photosynthetic parameters ($rETR_{max}$, α, I_k) estimated from PAM measurements on the field, to avoid over- or underestimation. To develop the tool, we used models previously designed by Kühl and Jørgensen (1992), Serôdio (2004) and Forster and Kromkamp (2004) by integrating the chl *a* distribution profiles and sediment granulometry from pure sand to pure mud. The sensitivity of the correction to sediment granulometry and the shape of chl *a* profile were evaluated theoretically using a typical fluorescence data set obtained using PAM measurements. Our results confirm the importance of accounting for both the chl *a* profile and sediment granulometry when estimating a light attenuation coefficient. We show that, with the same chl *a* profile, the photosynthetic parameters are more underestimated in mud than in a sandy environment. Thus, granulometry and the chl *a* profile need to be systematically quantified and used to correct raw data measured in field studies using PAM before estimating photosynthetic parameters. The numerical tool is available as an e-document that is simple and easy to apply to any PAM data.

1. Introduction

Littoral areas of lakes and coastal seas are among the most productive ecosystems in the world, and their production far exceeds that of open oceans (Geider et al., 2001). One of the main primary producers in these regions is the microalgae that develop in the euphotic zone of many types of benthic substrates (Underwood and Kromkamp, 1999; Aberle-Malzahn, 2004). The importance of microphytobenthic primary production (PP) is similar to that of phytoplankton (Underwood and Kromkamp, 1999) where ~90% of production is consumed or recycled to maintain local heterotrophic metabolism (Cloern et al., 2014). Many authors consider that the productivity and biomass of microphytobenthos (MPB) are greater than those of phytoplankton on intertidal mudflats (De Jonge and Van Beuselom, 1992; Lucas and Holligan, 1999; Guarini et al., 2000; Kang et al., 2015). Moreover, these microphytobenthic communities, which include assemblages of diatoms, green algae, and cyanobacteria (Admiraal et al., 1985) also have major ecological implications as ecosystem engineers (Sutherland et al., 1998; Tolhurst et al., 2006; Lubarsky et al., 2010), as trophic support for benthic fauna locally (Herman et al., 2000), but also after exports to adjacent habitats of intertidal mudflats (Ubertini et al., 2012; Kang et al., 2015).

The primary production and standing stocks of MPB biofilms inhabiting intertidal sediments vary at several spatial and temporal scales (Blanchard et al., 2001; Orvain et al., 2012). Changes can vary from very short to long time scales linked to tidal rhythm, daily photoperiod, spring/neap cycles and seasonal cycles (Taylor, 1964; Pinckney and Zingmark, 1991; Blanchard et al., 2001). Primary production also displays a high degree of spatial variability from high-resolution patchy distribution related to the intrinsic autoecology of biofilms (Weerman et al., 2011) to benthic fluxes regulated by macrofauna, biogeochemical components affecting organic matter, and release of nutrients (Thrush et al., 2013). But primary production is also influenced by mesoscale patterns related to the morphodynamics of estuarine landscapes and

* Corresponding author.
E-mail address: francis.orvain@unicaen.fr (F. Orvain).
[1] These authors contributed equally to this work.

https://doi.org/10.1016/j.jembe.2018.02.007
Received 12 June 2017; Received in revised form 23 February 2018; Accepted 25 February 2018
Available online 07 April 2018
0022-0981/

tidal bars and flats (Fagherazzi et al., 2014) and large scale changes related to sediment composition, salinity, nutrient inputs linked to river flows (Benyoucef et al., 2014) and shear stress (Fagherazzi et al., 2014). Among all these sources of variability, light is the main factor influencing primary production (Underwood and Kromkamp, 1999). There are major spatial and temporal gradients in the availability of light in MPB habitats that control primary production. Steep irradiance gradients occur across the surface of the sediment bed that depends on grain size (Kühl et al., 1994) and on the relative proportion of silt and sand. Intertidal sites are subject to varying patterns of diel lightning periods mediated by periods of tidal immersion (Underwood and Kromkamp, 1999). Such changes are accompanied by a variation in the spectral quality of light in sediments (Kühl and Jørgensen, 1992). Irradiance is further modified by increased attenuation of light at depth due to the presence of microalgal biofilms in the surface layers of the sediments (Ploug et al., 1993; Kühl and Jørgensen, 1994). To cope with light variability, the majority of epipelic microphytobenthos are mobile and undertake rhythmic vertical migration linked to both the diel and tidal cycles (Taylor, 1964; Baillie and Welsh, 1980; Edgar and Pickett-Heaps, 1984; Mitbavkar and Anil, 2004). In intertidal sediments, this motility has been hypothesized to be a strategy developed by MPB biofilms to colonize the illuminated surface when light is available (using upward migration). Downward MPB migration occurs during high exposure (tidal diurnal emersion), as a strategy to avoid photoinhibition due to high light exposure and potential saturation of photosystems (Admiraal, 1984) and to capture remineralized nutrients concentrated in deeper sediment layers (Orvain et al., 2003). The level of light at the surface of intertidal mudflats is very much higher than the highest possible level in the phytoplanktonic photic layer in the water column, the migratory strategy could thus be the main adaptation to limit impairment due to excessive light. Especially compared with other forms of physiological adaptation of diatom cells, such as modifications in internal chl *a* concentration, pigment composition, the number of active reactional centers, the size of the light harvesting cross section, or activation of xanthophyll cycle (Serôdio et al., 2012; Cartaxana et al., 2013). In diatoms, this mobility is associated with the excretion of extracellular polymeric substances (Decho, 2000), primarily glycoproteins, which can also be used by bacteria, meiofauna and macrofauna as carbon sources (Middelburg et al., 2000) and reinforce the importance of microphytobenthos as a food web support.

Because of high variability at short spatial and temporal scales, accurate measurements of primary productivity require rapidly repeated spatially and temporally close measurements while avoiding disturbances in the microscopic gradient of the photic zone under the air-sediment interface (Kühl and Jørgensen, 1994). However, traditional primary production measurements using labeled ^{14}C carbon cannot be used without disturbing natural assemblage and resuspending them in incubators for experiments longer than 1 h (Blanchard et al., 1996; Underwood and Smith, 1998). The turbidity and shading effects of algae make the control of light and its availability for algal cells difficult to accurately estimate in incubators. Moreover, the typical high-resolution variability of benthic primary producers and processes under the influence of natural microscopic gradients in the photic zone cannot be measured by such techniques. For this reason, there has been an increase in research on rapid non-intrusive methods using oxygen electrodes (Serôdio, 2003) and pulse amplitude modulated (PAM) fluorescence (Kromkamp et al., 1998; Serôdio, 2003; Forster and Kromkamp, 2004; Jesus et al., 2006), which exploits the optical properties of chlorophyll *a* pigments (chl *a*) for rapid and remote detection of the MPB photosynthetic activity in these fragile environments (Jesus et al., 2006). This technique has considerable advantages, such as the rapidity and non-intrusive nature of the measurements that facilitate adaptation to the degree of temporal and spatial variability of the MPB communities (Serôdio, 2004). PAM techniques are easily deployed in the field, explaining why there is extensive literature on the use of PAM fluorometers (Walz, Germany) in studies of MPB communities (Serôdio et al., 1997, 2007; Kromkamp et al., 1998; Underwood and Kromkamp, 1999; Barranguet and Kromkamp, 2000; Serôdio and Catarino, 2000; Perkins et al., 2001, 2011; Forster et al., 2006; Vieira et al., 2013; Juneau et al., 2015).

The PAM method relies on measurements of the fluorescence emitted by MPB in response to light pulses. After a period of darkness imposed on the MPB sample (between 5 and 10 min depending on the study), the minimum level of fluorescence (F_0) is recorded. Then, in response to a light saturating flash, the maximum level of fluorescence (F_M) is recorded. After which increasing the pulse of actinic light (I) with a time lag (e.g. lasting 30 s) makes it possible to measure a series of steady-state fluorescence level $F_S(I)$ and new maximum levels $F_M'(I)$. Using these fluorescence values, the light level (I) and an ETR factor, the electron transport rate (ETR) in photosystem II (PSII), which equals the product of apparent or effective photochemical efficiency, can be calculated: $ETR(I) = [(F_M'(I) - F_S(I)) / F_M'(I)] \times I \times$ ETR factor. Since the percentage of photons absorbed by active Photosystem II (PSII) is debatable and can differ among species according to Johnsen and Sakshaug (2007) and Schreiber et al. (2012), the ETR factor is not considered as a constant value. During the first steps of data treatment of PAM results, ETR can be expressed in relative form: $rETR(I) = [(F_M'(I) - F_S(I)) / F_M'(I)] \times I$. Photosynthetic parameters ($rETR_{max}$, α, I_{opt} and I_k) can therefore be estimated by adjusting the rETR/I curves to photosynthetic non-linear models: for instance either the Webb et al. (1974) model, when there is no decrease in rETR at high levels of I, or the Eilers and Peeters (1988) model, when there is an apparent decrease in rETR at the highest I. Although these method do not allow direct access to primary production measurements, many studies have shown that it is possible to use the fluorescence approach to estimate primary production as accurately as with other traditional incubation methods, such as carbon incorporation or oxygen release measurements (Hartig et al., 1998; Barranguet and Kromkamp, 2000; Serôdio, 2003; Morris and Kromkamp, 2003; Serôdio et al., 2007).

However, PAM measurements require cautious interpretation especially because of the micro-heterogeneity of the benthic habitat, which has marked effects on light and fluorescence attenuation in sand and mud particles (Kühl and Jørgensen, 1994) and vertical profiles of the MPB biomass (Vieira et al., 2013), but also because of the microtopography that affects incident light at the surface. Thus PAM measurements are actually affected by light attenuation, which in turn, is mainly dependent on the vertical profile of chl *a* concentration (self-shading by the MPB positioned in the upper layers), their migration behavior, and grain size (Kühl and Jørgensen, 1994; Forster and Kromkamp, 2004; Serôdio, 2004), but also by minor factors like the effect of the different composition of pigment in the MPB species assemblage (diatoms, cyanobacteria, euglenoids) on spectral radiation, the presence of pheopigment, which are breakdown products of chl *a*, and the presence of water (Kühl and Jørgensen, 1994). Perkins et al. (2011) argued that the application of chlorophyll fluorescence to MPB biofilms is complex because of the signal emanating from subsurface cells, vertical cell migration in the sediment matrix, high regulation capacity, chlororespiration in the dark, and the effects of the physical structure of the sediment/biofilm matrix (light attenuation caused by the sediment matrix). Due to light attenuation in the sediment, the level of irradiance received by the photosynthetic cells in their vertical position in the sediment photic layer is attenuated. Conversely, the attenuation also affects the fluorescence returned by cells and measured at the surface of the sediment. For these reasons, raw field measurements underestimate the actual level of fluorescence produced. Serôdio (2004) and Forster and Kromkamp (2004) demonstrated that it is possible to calculate light and fluorescence attenuations during PAM measurements. These two studies agreed that 40% of the error in estimations of photosynthetic parameters occurs between measured and corrected values. These models were applied in case studies (scenarios) by simulating various vertical migratory patterns with the microscopic profile of chl *a* biomass. However, the granulometry of the sediment

can also modify light availability for diatoms under the surface of the sediments (Kühl and Jørgensen, 1994; Kühl et al., 1994; Jesus et al., 2005), but the wide range of natural situations encompassing all types of sand-mud mixtures (from pure mud to pure sand) has never been taken into account in the corrections.

In the present study, the model developed by Serôdio (2004) and Forster and Kromkamp (2004) was updated into a new data processing tool that can be applied to field measurements to better evaluate in situ microphytobenthic photosynthetic parameters, and subsequently, primary production. The sensitivity of the tool was tested in various types of microalgal distribution (chl *a* vertical profile) and of sediment granulometry, ranging from pure mud to pure sand. Conclusions about the importance of the application of this correction for accurate estimation of microphytobenthos photosynthetic parameters are thus put forward. The practical numerical tool can be used to readjust photosynthetic parameters of in situ measurements in routine applications. All the algorithms were performed using Excel (see e-document) and Matlab (available on request).

2. Methods

2.1. Step-by-step details of irradiance/fluorescence correction from PAM measurements in sediment biofilm

2.1.1. Light attenuation coefficient

The term 'light' (as well as irradiance) in the following paragraphs refers to ambient photosynthetically active radiation (PAR). To estimate the light attenuation with depth in the foreshore sediment, a light attenuation coefficient (Table 1; k_d; mm^{-1}) was calculated using the equation provided by Forster and Kromkamp (2004). This equation takes into account the sediment dry weight (PSed) at each depth interval (z_i), their specific attenuation value $k^*_{d(sed)}$, the proportion of chl *a* content (PChl *a*) and their specific attenuation coefficient $k^*_{d(chl\ a)}$, as:

$$k_{d(zi)} = (PSed_{zi} \times k^*_{d(sed)}) + (PChl_{zi} \times k^*_{d(chl\ a)}) \quad (1)$$

PChl *a* was calculated for each section from cumulative chl *a* concentration ($mg\,m^{-2}$) from the surface to the depth (z_i) of the section concerned according to the equation:

$$PChl\ a_{z_i} = \frac{\frac{\text{cumulative Chl}a\,(z_i)}{-z_i}}{2.9} \quad (2)$$

where z_i is the depth of the section in µm, assuming a theoretical maximum areal chl *a* concentration of $29\,mg\,m^{-2}$ for a depth of 10 µm (Forster and Kromkamp, 2004), and $2.9\,mg\,m^{-2}$ for a depth of 1 µm. We decided to use the same value as Forster and Kromkamp (2004), which is a little higher than the $25\,mg\,m^{-2}$ of areal chl *a* concentration estimated by Guarini et al. (2000) in their dynamic model of MPB primary production. The cumulative chl *a* ($mg\,m^{-2}$) was calculated directly from the chl *a* content of each interval from vertical profiles (chl a_{zi}; $\mu g\,gDW^{-1}$). These values of chl *a* were obtained by sampling minicores in the field and immediately freezing them. Each section was then sliced with a cryotome to measure dry mass and chl *a* content. The conversion from $\mu g\,gDW^{-1}$ to $mg\,m^{-2}$ was based on the dry bulk density ($g\,cm^{-3}$) and the depth of the section (mm). The fractions $PSed_{zi}$ (Eq. (1)) were calculated according to the relation: $PSed_{zi} = 1 - Pchl_{zi}$.

The reference value for chl *a* specific attenuation coefficient of $0.02\,m^2\,mg\,chl\,a^{-1}$ (Forster and Kromkamp, 2004) was used to estimate the attenuation coefficient, $k^*_{d(chl\ a)}$ (Eq. (1)), and a value of $58\,mm^{-1}$ was obtained ($k^*_{d(chl\ a)} = 2.9\,mg\,chl\ a\,m^{-2}\,\mu m^{-1} \times 0.02\,m^2\,mg\,chl\,a^{-1} = 58\,mm^{-1}$). The reference value of specific attenuation coefficient of $0.02\,m^2\,mg\,chl\ a^{-1}$ was originally based on the table of values for planktonic diatom cells in Kirk (1983) and confirmed for microphytobenthic diatoms by Forster and Kromkamp (2004)

The reference value for sediment specific attenuation coefficient of $0.011\,m^2\,mgDW^{-1}$ enabled us to obtain a value of $2\,mm^{-1}$ for $k^*_{d(sed)}$ (Eq. (2)) in absence of chl *a* (Forster and Kromkamp, 2004). However, in a mixture of sand and mud, the value of $k^*_{d(sed)}$ can change with changes in the grain-size composition of sediments (Kühl and Jørgensen, 1994) thereby changing k_{di} values. In the same way that the

Table 1
Explanations of the photophysiological parameters and notations used in this study.

Parameters	unIt	Explanation
I, I_0	$\mu mol\ photons\,m^{-2}\,s^{-1}$	- Irradiance at the surface (Photosynthetically active radiation)
I_{zi}		- Irradiance at the depth z_i (Photosynthetically active radiation)
I_{opt} or $I_{opt\text{-}c}$		- Optimal Irradiance for photosynthesis obtained with rETR/I curves (Eilers and Peeters, 1988) before and after correction (c)
I_k or $I_{k\text{-}c}$		- Light saturation index before and after correction (c)
F_0	No units	- Minimum fluorescence emitted by a dark-adapted sample (I = 0)
F_M		- Maximum fluorescence emitted by a dark-adapted sample (I = 0)
F_S	No units	- Steady-state fluorescence emitted by a light-adapted sample (I)
F_M'		- Maximum fluorescence emitted by a light-adapted sample (I)
F_{SE}	No units	- Fs emitted ($_E$) by microphytobenthos pigments
F_{SR}		- Fs received ($_R$) by the PAM sensor after attenuation of F_{SE}
F_{ME}		- F_M emitted ($_E$) by microphytobenthos pigments
F_{MR}		- F_M received ($_R$) by the PAM sensor after attenuation of F_{ME}
F(I;z)	No units	- Fluorescence for an irradiance I and a depth z
F_{MET}	No units	- Total F_{ME} from all interval of depth
F_{SET}		- Total F_{SE} from all interval of depth
F_{MRT}		- Total F_{MR} from all interval of depth
F_{SRT}		- Total F_{SR} from all interval of depth
k_d	mm^{-1}	- Light attenuation coefficient
$k^*_{d(sed)}$		- specific attenuation coefficient of the sediment particles
$k^*_{d(chl\ a)}$		- specific attenuation coefficient of the chl *a* pigment
(r)ETR(I)	$\mu mol\ electrons\,m^{-2}\,s^{-1}$	- (Relative) electron transport rate obtained with PAM measurement
$rETR_{max}$		- Maximum rETR(I) measured with rETR/I curves (Eilers and Peeters, 1988) before and after correction (c)
$rETR_{max\text{-}c}$		
z_i	mm	- Depth of a sediment layer interval (i)
z_{max}		- Maximum depth where fluorescence is detected
α	$\mu mol\ electrons\ (\mu mol\ photons)^{-1}$	- Maximum light efficiency measured with rETR/I curves (Eilers and Peeters, 1988) before and after correction (c)
α_c		
δ	%	- Percentage of correction after model application
NPQ(I)	Fluorescence ratio	- Non-photochemical quenching

variation in chlorophyll has to be taken into account, so does variation in sediment composition. In this study, the $k^{*}_{d(sed)}$ was not considered as a constant value but was changed as a function of the granulometry (See Methods. 2.2 Model sensitivity to sediment granulometry).

2.1.2. Irradiance correction

The irradiance from ambient photosynthetically active radiation (PAR) as well as artificial light emitted by the PAM fluorometer and discerned by the microphytobenthos can be considered as an attenuated beam from above due to the successive layers of sediment and the superficial biofilms according to the previously calculated attenuation coefficient k_d (Eq. (1)). Actual irradiance as detected by deep MPB cells can be expressed at each distance from the surface using the Beer-Lambert equation as:

$$I_{zi} = I_0 \times e^{kd_{(zi)} \times z_i} \quad (3)$$

where I_0 is the irradiance at the surface in µmol photons $m^{-2} s^{-1}$, z_i (mm) the depth of the section considered and $k_{d(zi)}$ is the light attenuation coefficient in mm^{-1} (Eq. (1)) at depth z_i.

2.1.3. Fluorescence correction

For an irradiance (I) sent by a PAM device (PAR), irradiance I_{zi} will be received by the MPB cells at depth z_i. In response, the photosynthetic apparatus of these cells emit fluorescence (hereafter, the suffix $F\text{-}_E$ for Emitted fluorescence will be used to express this level). This level of fluorescence is attenuated for the same reason as that of irradiance, but in this case, from a signal coming from the depth before being measured by the PAM device (hereafter the suffix $F\text{-}_R$ for Received fluorescence will be used to express this level).

As PAM sends a "measuring light" to estimate the minimum fluorescence (F_0), different intensity pulses of saturating light to estimate maximum fluorescence values (F_M or F_M') and actinic lights to estimate steady-state fluorescences (F_S) (Van Kooten and Snel, 1990). Using the measured fluorescence, the PAM method makes it possible to estimate a relative electron transport rate (rETR; µmol electrons $m^{-2} s^{-1}$) for each level of actinic irradiance (I; µmol photons $m^{-2} s^{-1}$) calculated as follows:

$$rETR(I) = \frac{F_M'(I) - F_S(I)}{F_M'(I)} \times I \quad (4)$$

Similar to irradiance, the fluorescence values used in Eq. (4) have to be corrected as a function of the real irradiance I_{zi} (Eq. (3)) received by the MPB cells and by considering the subsequent attenuation of fluorescence along the sediment layers.

The polynomial trend line of the F_S (and F_M) versus I curves measured by the PAM device at surface was plotted and fitted to extract the coefficients (*a*, *b*, *c* and *d*) of the polynomial regression (Fig. 1).

Then, for each I_{zi} and z_i, the steady-state fluorescence emitted by the microphytobenthos $F_{SE}(I_{zi}; z_i)$ was calculated with the polynomial coefficients as:

$$F_{SE}(I_{zi}; z_i) = (a \times I_{zi}^3 + b \times I_{zi}^2 + c \times I_{zi} + d) \times \frac{I_{zi} \times Chl\ a(z_i)}{I_T} \quad (5)$$

where I_T represents the cumulative I_{zi} received and used by the chl *a* content (mg chl *a* m^{-2}) for each interval (di) calculated as follows:

$$I_T = \sum_i (I_{zi} \times chl\ a(z_i) \times di) \quad (6)$$

The steady-state fluorescence measured by the PAM ($F_S = F_{SR}$) corresponds to the integration of the F_{SE} values after attenuation by the layers of sediment and the biofilms (Fig. 2). The $F_{SR}(I_{zi}; z_i)$ values represent the attenuated $F_{SE}(I_{zi}; z_i)$ values along the depth layers according to the attenuation coefficient k_d previously calculated (Eq. (1)) and can be calculated for each depth z_i as:

$$F_{SR}(I_{zi}; z_i) = Fse(I_{zi}; z_i) \times e^{kd_{zi} \times z_i} \quad (7)$$

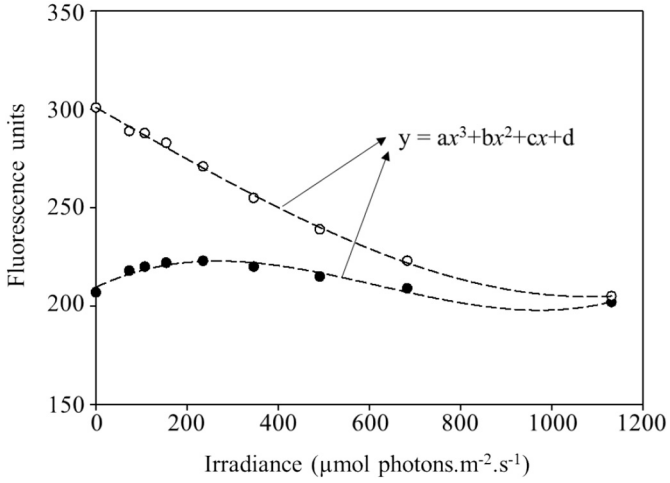

Fig. 1. Plot of the stable (F_S; black dots) and maximum (F_M; empty circles) fluorescence values as a function of the different irradiance values sent by the PAM device (ordinates). Values were chosen as a function of the curve profile and obtained from PAM measurement performed on MPB biofilm from an intertidal mudflat (Baie des Veys, France). The relations were fitted using a polynomial trend ($y = ax^3 + bx^2 + cx + d$) to estimate the F_{SE} and F_{ME} values using the real irradiance received by the cells (I_{zi}).

The steady-state fluorescence emitted by the MPB in one deep layer is estimated by considering that the fluorescence received is attenuated (Equation in Fig. 2). The actual emitted steady-state fluorescence (F_{SE}) after attenuation (F_{SR}) can then be estimated (see e-document). Thus, the F_S values measured by the PAM device for a given irradiance I, represent the integration over depth of the Total Received Fs from the different layers as:

$$F_{SRT}(I) = \int_0^{z_{max}} F_{SR}(I_{zi}; z_i) di \quad (8)$$

where z_{max} is the maximum depth at which the microphytobenthos can detect the downwelling beam of irradiance under the surface and *di* is the interval of depth where the fluorescence was emitted by chl *a* pigments.

In the dark ($I = 0$), the fluorescence values $F_{SE}(I_0,z_i)$ cannot be evaluated with the previous method used to calculated the other F_{SE}, relying on irradiance. To get round this problem, the $F_{SE}(I_0,z_i)$ values were extrapolated from the three-order polynomial trend lines of $F_{SE}(z_i)$ versus I_{zi} curves and considered to be equal to the coefficient *d* from the polynomial trend ($y = ax^3 + bx^2 + cx + d$) (Fig. 3).

Due to the effects of light attenuation, the value F_{SRT}, which should be equal to the F_S initially measured by the PAM device, is higher. Thus, for each $F_S(I)$, a coefficient ω(I) was calculated (Eq. (9)) and each value of $F_{SE}(I_{zi}; z_i)$ and $F_{SR}(I_{zi}; zi)$ was corrected (Eqs. (10) & (11)):

$$\omega(I) = \frac{F_{SRT}(I)}{F_S(I)} \quad (9)$$

$$F_{SE}(I_{zi}; z_i)c = F_{SE}(I_{zi}; z_i) \times \omega(I) \quad (10)$$

$$F_{SR}(I_{zi}; z_i)c = F_{SE}(I_{zi}; z_i)c \times e^{kd_{zi} \times z_i} \quad (11)$$

The same steps as those described for F_S (Eqs. (5) to (11)) were applied to the fluorescence values of F_M'.

All these calculations allowed us to access the fluorescence values that are emitted by the MPB cells before attenuation (F_{SE} and F_{ME}) and can now be used to calculate the rETR(I) actually emitted (rETRc) either for each depth interval ($rETRc(I_{zi}; z_i)$; Eq. (12)), or for the entire profile (rETRc(I); Eq. (13)).

$$rETRc(I_{zi}; z_i) = \frac{F_{ME}(I_{zi}; z_i)c - F_{SE}(I_{zi}; z_i)c}{F_{ME}(I_{zi}; z_i)c} \times I_{zi} \quad (12)$$

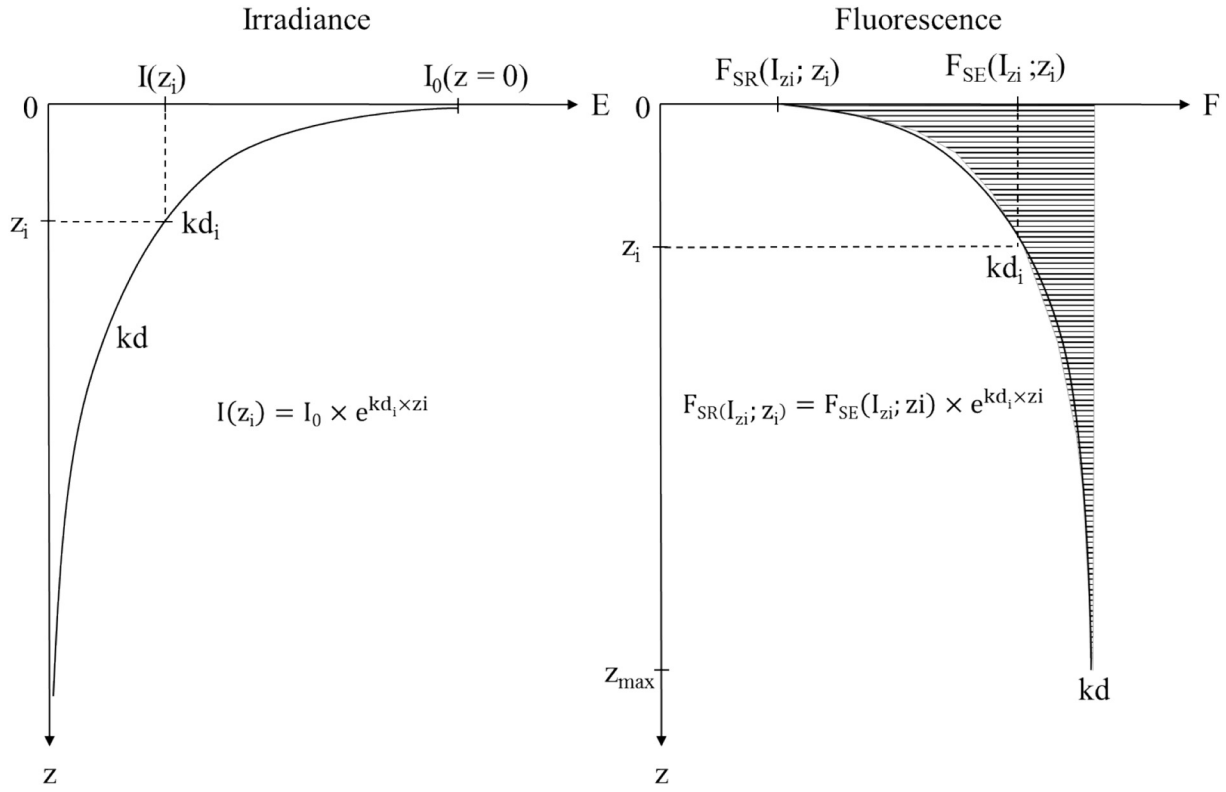

Fig. 2. Illustration of the terms used in Eqs. (3), (5) and (7). The irradiance received at each depth z_i (I_{zi}) by the microphytobenthic cells is an attenuated value compared with the real irradiance at the surface (I_0) following a light attenuation coefficient (k_d) which can differ with the light, biomass distribution and the type of sediment. In the same way, the level of fluorescence, $F_{SR}(Iz_i; z_i)$, at the surface is an attenuated value compared with the real fluorescence emitted by undisturbed microphytobenthos biofilms $F_{SE}(Iz_i; z_i)$ from depth following the same attenuation coefficient.
(Figure taken from Serôdio (2004) and modified)

$$rETRc(I) = \frac{F_{MET}(I)c - F_{SET}(I)c}{F_{MET}(I)c} \times I \quad (13)$$

After the spectral quality of k_d is taken into consideration, the fluorescence attenuation is higher than the light attenuation, as shown by Kühl et al. (1994). Thus, Serôdio (2004) considered separated values of attenuation coefficients for irradiance and fluorescence. In this study, following the approach used by Forster and Kromkamp (2004), we decided not to use different values of fluorescence and light attenuation because the fluorescence values were estimated as a function of irradiance values by using a polynomial equation (Figs. 2 & 3) that actually included these spectral differences.

2.1.4. rETR vs. I curves

Each originally measured rETR(I), and each rETRc(I) estimated after correction, were plotted as a function of the initial levels of irradiance sent (I). To estimate the photosynthetic parameters, the mechanistic model of Eilers and Peeters (1988) (Eq. (14)) was applied and the coefficients (*a*, *b*, *c* and *d*) of each fit were extracted:

$$rETR(I) = \frac{I}{(aI^2 + bI + c)} \text{ and } rETRc(I) = \frac{I}{(a_cI^2 + b_cI + c_c)} \quad (14)$$

Next, the photosynthetic parameters were calculated. Using the maximum light utilization efficiency (α; Eq. (15)), the maximum photosynthetic capacity ($rETR_{max}$; Eq. (17)) and the light saturation index (I_k; Eq. (18)) were calculated before and after correction (subscript c) as follows:

$$\alpha = \frac{1}{c} \text{ and } \alpha_c = \frac{1}{c_c} \quad (15)$$

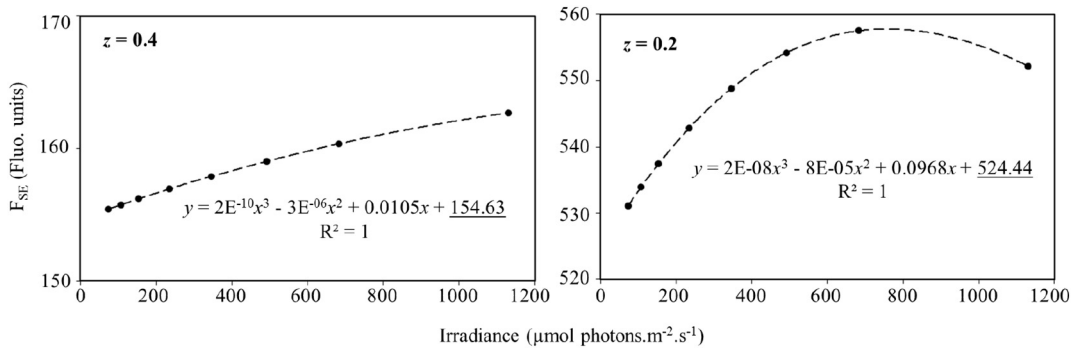

Fig. 3. Plot of the steady state fluorescence (F_{SE}; black dots) emitted as a function of the different irradiance values sent by the PAM device (ordinates) for a defined depth ($z = -0.2$ mm at the top and $z = -0.4$ mm at the bottom). The relations were fitted using a polynomial trend ($y = ax^3 + bx^2 + cx + d$) to estimate the F_{SE} values for I = 0 considered as equal to the coefficient d from the polynomial trend.

$$I_{opt} = \sqrt{\frac{1}{\alpha \times a}} \text{ and } I_{opt-c} = \sqrt{\frac{1}{\alpha_c \times a_c}} \quad (16)$$

$$rETR_{max} = \frac{1}{b + \frac{2}{\alpha \times I_{opt}}} \text{ and } rETR_{max-c} = \frac{1}{b_c + \frac{2}{\alpha_c \times I_{opt-c}}} \quad (17)$$

$$I_k = \frac{rETR_{max}}{\alpha} \text{ and } I = \frac{rETR_{max-c}}{\alpha_c} \quad (18)$$

2.1.5. Non-photochemical quenching

The corresponding heat dissipation of the excess absorbed light energy, which can be estimated from the non-photochemical quenching (NPQ) of chl *a* fluorescence (Serôdio and Lavaud, 2011; Chukhutsina et al., 2014), can also be calculated before attenuation either for each depth interval ($NPQ(I_{zi}; z_i)c$; Eq. (19)), or for the entire profile ($NPQ(I)c$; Eq. (20)):

$$NPQ(I_{zi}; z_i)c = \frac{F_{ME}(I = 0; z_i)c - F_{ME}(I_{zi}; z_i)c}{F_{ME}(I_{zi}; z_i)c} \quad (19)$$

$$NPQ(I)c = \frac{F_{MET}(I = 0)c - F_{MET}(I)c}{F_{MET}(I_{zi})c} \quad (20)$$

All these calculations enabled access to the actual photosynthetic parameters of microphytobenthic cells that were subject to light attenuation and received fluorescence signals emitted by sediment grains and chlorophyll along the depth profile. All these calculations are made by a rapid automatic correction tool in which the user can change the raw values to apply the same correction. This tool is now available as an Excel file (see e-document) or Matlab script (available on request).

2.2. Model sensitivity to sediment granulometry

As mentioned above, the $k^*_{d(sed)}$ and the shape of chl *a* should not be considered as constant values when $k_{d(zi)}$ are estimated (Eq. (1)). To emphasize this, the sensitivity of the correction tool to $k^*_{d(sed)}$ variability and the shape of the chl *a* profile was evaluated in theoretical study cases.

A typical fluorescence data set exhibiting an apparent decrease at high irradiance was used (Table 2) but the tool developed in this study is available for each fluorescence data set. The polynomial trends of this fluorescence dataset ($ax^3 + bx^2 + cx + d$; Fig. 1) used in Eq. (5) were estimated and the coefficients extracted: for F_S ($a = -3.97 \times 10^{-8}$; $b = -2.87 \times 10^{-6}$; $c = -0.13$; $d = 301.04$; $R^2 = 0.997$) and F_M ($a = 1.42 \times 10^{-7}$; $b = -0.0003$; $c = 0.11$; $d = 209.56$; $R^2 = 0.910$).

To account for the chl *a* specific "self-shading" of the light attenuation, different types of chl *a* depth profiles were tested (Fig.4). The proposed profiles of chl *a* distribution are representative of typical situations. Indeed, chl *a* depth profiles can change on intertidal flats. First, we propose a uniform vertical distribution (Fig. 4-1) typical of sandier sites, but that also occurs in recently deposited fluid layers of mud. Second, a distribution with strongly accumulated chl *a* in the uppermost 500 µm layer (Fig. 4-3) observed in muddier sites (Kühl and Jørgensen, 1992; Barranguet and Kromkamp, 2000; Jesus et al., 2006) mainly in the middle of the diurnal immersion period in sunny conditions (Dupuy et al., 2014). Third, at the beginning and at the end of immersion periods (the first and last 30 min), MPB chl *a* in muddy sediments has been shown to be more concentrated in subsurface layers (with a peak at 1–2 mm; Fig. 4-2) and this situation is also encountered in the middle of immersion periods, in the case of rainfall (Tolhurst et al., 2003). In nature, MPB biofilm can tend to migrate downward very rapidly during immersion periods, when rain is falling (Perkins et al., 2003). The typical scheme of MPB migration is clearly responsible for these succeeding steps of chl *a* vertical distribution (Serôdio et al., 1997; Blanchard et al., 2001; Orvain et al., 2003).

Table 2
A reference data set of PAM measurements exhibiting an apparent decrease at a high level of irradiance (> 400 µmol photons $m^{-2} s^{-1}$). Values were chosen as a function of the curve profile and obtained from PAM measurements performed on MPB biofilms from an intertidal mudflat (Baie des Veys, France). I is the irradiance perceived by the sample, F_S is the steady-state fluorescence and F_M the maximum fluorescence measured at each irradiance.

I	0	73	107	154	235	346	491	683	1131
F_S	207	218	220	222	223	220	215	209	202
F_M	301	289	288	283	271	255	239	223	205

The light attenuation coefficients for non-colonized sediments were measured by Kühl and Jørgensen (1994) on sediments ranging from wet sand to pure mud. The values estimated for different particle sizes of > 63, 63–125, 125–250 and 250–500 µm, were 3.46, 1.64, 1.60 and 0.99 mm^{-1}, respectively. To account for the influence of variation in the sediment specific attenuation $k^*_{d(sed)}$ in numerical simulations, we used a minimum value of 1 mm^{-1}, representative of low attenuation in sandy sediments, and a maximum value of 4 mm^{-1}, representative of high attenuation in muddy sediments. These values are close to the values found by Kühl and Jørgensen (1994) for dry sand and diatoms. The degree of compaction can also alter the attenuation coefficient due to rapid variations in water content caused by consolidation during periods of immersion (Jesus et al., 2006).

Six theoretical scenarios were tested by crossing the 2 factors: $k^*_{d(sed)}$ and the shape of the chl *a* profile (Table 3).

3. Results

In all the case studies, the corrected rETR values (rETRc) were consistently higher than those measured initially, revealing underestimation of this parameter in the absence of correction. In comparison, the corrected NPQ was not affected by the correction, with a

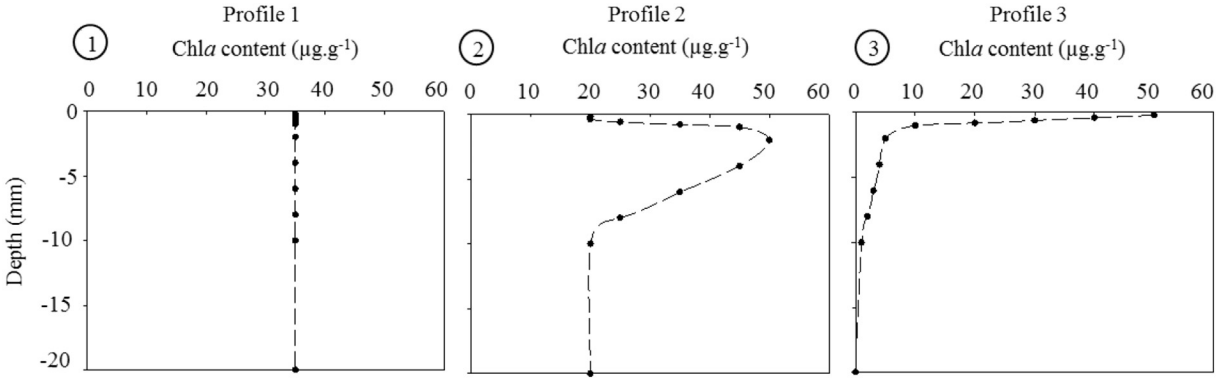

Fig. 4. Profiles of the vertical distribution of chlorophyll *a* used in the theoretical simulation of the fluorescence correction with a linear profile (1), a profile with a peak of chl *a* at −2 mm from the surface (2), and a profile with an established MPB biofilm at the surface (3).

Table 3
Characterization of the six different scenarios used in the exercises to check the sensitivity of the correction model. With potential minimum ($1\,mm^{-1}$) and maximum ($4\,mm^{-1}$) values for the sediment specific attenuation coefficient ($k^*_{d(sed)}$) and three typical profiles of chl *a* content (Fig. 4).

Scenario	Value of $k^*_{d(sed)}$	Typical chl *a* profile
1	1	Homogeneous (Fig. 4-1)
2	4	Homogeneous
3	1	Subsurface peak (Fig. 4-2)
4	4	Subsurface peak
5	1	Established MPB biofilm (Fig. 4-3)
6	4	Established MPB biofilm

typical saturation effect in response to excessive light by following a sigmoidal pattern (Fig. 5).

Regarding photosynthetic efficiency (α; μmol electrons $m^{-2}\,s^{-1}$ (μmol photons $m^{-2}\,s^{-1})^{-1}$), the highest correction was estimated for a chl *a* biomass peak 2 mm under the sediment surface (profile 2) and for both $k^*_{d(sed)}$: 39.04% in sand (scenario 2; $k^*_{d(sed)} = 1\,mm^{-1}$) and 53.11% in mud (scenario 5; $k^*_{d(sed)} = 4\,mm^{-1}$). The lowest correction of α was estimated for an established MPB biofilm (profile 3), which colonized the top 1000 μm layer with a steep chl *a* gradient (scenario 3 in the sand with 19.09% and scenario 6 in the mud with 39.13%). A significant correction for α was then observed with a mean corrected value that was 38.98 ± 10.86% higher than the raw value. Corrected α values were always higher than measured values (Table 4), thereby confirming underestimation of photosynthetic efficiency in the absence of correction. Considering $k^*_{d(sed)}$ was very important for the correction of α which showed corrected values from 13.90 to 20.05% higher in the mud than in the sand (Table 5).

Regarding the maximum relative electron transport rate ($rETR_{max}$; μmol electrons $m^{-2}\,s^{-1}$), the smallest correction (Table 4; 12.23%) was observed for the sandy environment with an established biofilm (scenario 3). The highest correction (39.11%) for a muddy environment was associated with a profile with a biomass peak at the subsurface (scenario 5). Although the two factors (chl *a* profile and $k^*_{d(sed)}$) played a significant role in estimating the $rETR_{max}$, the fluorescence correction for this parameter was more sensitive to the vertical pattern of chl *a* than to the $k^*_{d(sed)}$ effect. In our simulation, the variation of $k^*_{d(sed)}$ led to a correction percentage as a function of the $k^*_{d(sed)}$ considered, which differed by from −1.25 to 3.42% (Table 5).

Regarding the light saturation coefficient (I_k; μmol photons $m^{-2}\,s^{-1}$), the correction percentage was lower after than before correction with a mean correction of −9.37 ± 5.50%. In contrast to other photosynthetic parameters, this result highlights underestimation of the light saturation coefficient in the absence of correction. The highest correction (−17.79%) was recorded in muddy sediment with an established MPB biofilm (profile 6; Table 4). The lowest (−2.41%) was recorded in sandy sediment with a biomass profile that culminated at the subsurface (profile 2; Table 4). In our simulation, the variation in $k^*_{d(sed)}$ led to a correction percentage as a function of the $k^*_{d(sed)}$ considered, which differed by from −6.73 to −12.03% (Table 5).

In all the scenarios, apparent photoinhibition (at saturating irradiances) was reduced to some extent, and sometimes completely (Fig. 5; scenario 5). In the first part of the rETR/I curves (< 200 μmol $h\nu \cdot m^{-2} \cdot s^{-1}$), the six simulations (either with or without correction) were very similar and the differences increased most with increasing irradiance values.

The correction tool made it possible to estimate the differences in terms of fluorescence of the different depth layers with the same surface irradiance. We chose to show the different rETR/I curves as a function of surface incident irradiance, rather than of the light actually received in deep layers, because our objective here is to apply the correction and to readjust the photosynthetic parameters for subsequent assessment of primary production. For the same incident light at the surface, the corrected values of photosynthetic parameters consider the fluorescence emitted by the cells in depth, at a higher level than the fluorescence received by the PAM optic fiber (Fig. 6). Indeed, with the same irradiance on the surface, each layer will receive a different attenuated irradiance and the fluorescence produced will also differ. This step is illustrated (Fig. 6) on the reference curve with an intermediate value of $k^*_{d(sed)} = 2\,mm^{-1}$ and with a typical structured MPB biofilm, which is

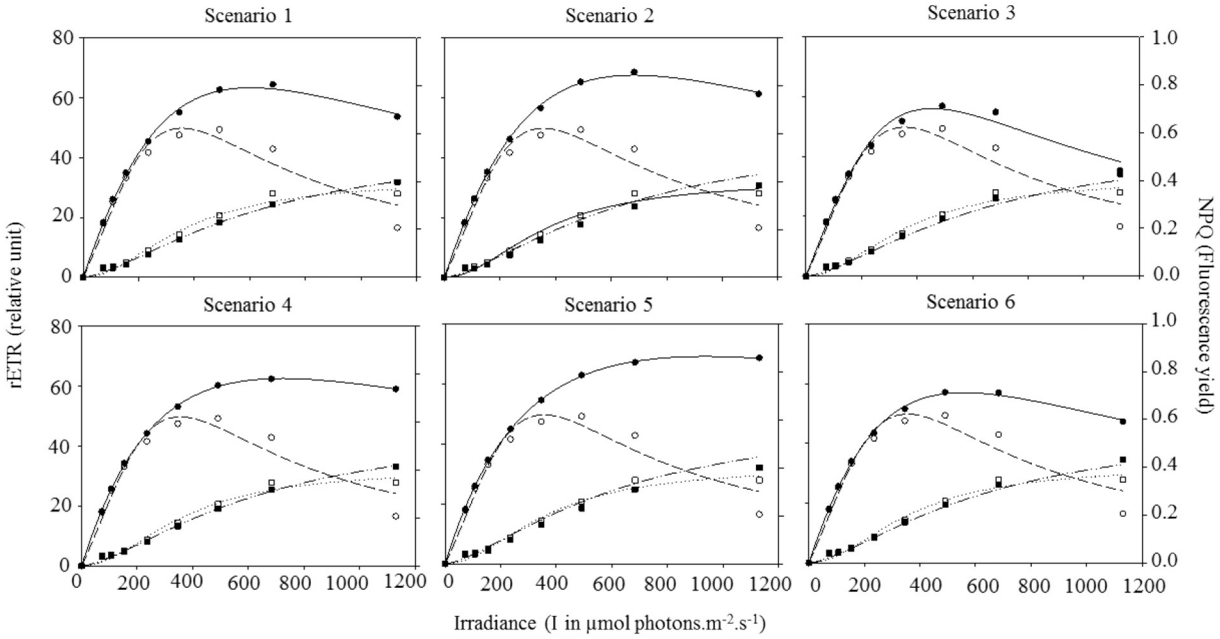

Fig. 5. Comparison of the general effects of correction on the light-response curves of rETR (circle; μmol electrons $m^{-2}\,s^{-1}$) and NPQ (square; fluorescence yield) curves in the 6 scenarios. The 6 scenarios were designed to compare the effect of the type of sediment (scenarios 1, 2, and 3 with sand ($k_d = 1\,mm^{-1}$), and scenarios 4, 5, and 6 with mud ($k_d = 4\,mm^{-1}$)) and the type of vertical profile of chl *a* biomass with a homogeneous profile (scenarios 1 & 4), a vertical profile with chl *a* peaking at subsurface layers (scenarios 2 & 5) and a constituted MPB biofilm peaking at the surface (scenarios 3 & 6). The curves are plotted to show the difference before (empty symbols) and after (lack dots) correction by the light-fluorescence attenuation model.

Table 4
Values of the photosynthetic parameters extracted using the Eilers and Peeters (1988) fit with photosynthetic efficiency (α), relative maximum electron transport rate (rETRmax) and optimal light for photosynthesis (Iopt; μmol photons $m^{-2} s^{-1}$) before and after correction. Variation coefficients (δ in %) of each parameter are given to enable evaluation of the difference before and after correction and their average values (±SD).

	Before correction			After correction					
Scenarios	α	$rETR_{max}$	I_k	α	δ_α	$rETR_{max}$	$\delta_{rETRmax}$	I_k	δ_{Ik}
1	0.20	49.85	250.52	0.27	34.79	63.35	27.08	236.17	−5.73
2				0.28	39.04	67.64	35.69	244.48	−2.41
3				0.24	19.09	55.95	12.23	236.08	−5.76
4				0.30	48.69	62.72	25.82	211.99	−15.38
5				0.30	53.11	69.35	39.11	227.62	−9.14
6				0.28	39.13	57.02	14.39	205.96	−17.79
Mean ± SD					38.98 ± 10.86		25.72 ± 9.92		−9.37 ± 5.50

Table 5
Percentage difference between the corrected values in sand (k_d = 1 mm^{-1}) and the corrected values in mud (k_d = 4 mm^{-1}). The percentages were calculated by subtracting the variation coefficient in sand (δ in %) from the variation coefficient in mud (Table 4).

Typical chl *a* profile	Scenarios	Differences between k_d = 1 and k_d = 4 mm^{-1}		
		α	$rETR_{max}$	I_k
Homogeneous (Fig. 2-1)	1 & 4	+13.90	−1.25	−9.66
Subsurface peak (Fig. 2-2)	2 & 5	+14.06	+3.42	−6.73
Established biofilm (Fig. 2-3)	3 & 6	+20.05	+2.16	−12.03

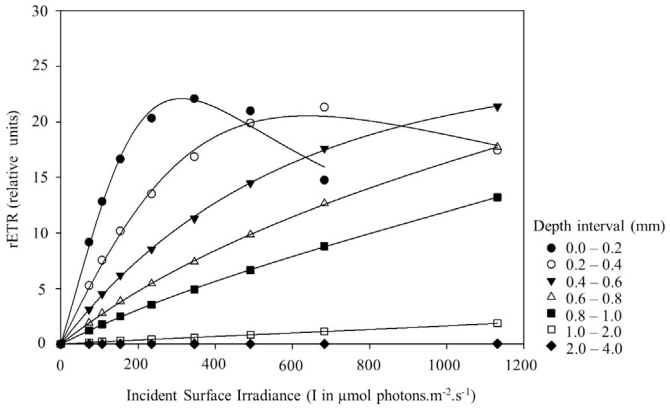

Fig. 6. Fine scale vertical pattern of light curves of rETR curves for an established biofilm and a moderate attenuation coefficient ($k^*_{d(sed)}$ = 2 mm^{-1}). Values of rETR (relative units) are plotted versus irradiance (μmol photons $m^{-2} s^{-1}$) at different depth intervals, from 0 to 0.2 mm to 2.0–4.0 mm (see legend).

Table 6
Values of the photosynthetic parameters extracted using the Eilers and Peeters (1988) fit with photosynthetic efficiency (α), relative maximum electron transport rate ($rETR_{max}$) and the optimal light for photosynthesis (I_{opt}; μmol photons $m^{-2} s^{-1}$) after application of our corrective model at each depth interval (mm).

Depth interval (mm)	0.0–0.2	0.2–0.4	0.4–0.6	0.6–0.8	0.8–1.0	1.0–2.0	2.0–4.0
α	0.117	0.072	0.043	0.027	0.017	0.002	0.000
$rETR_{max}$	22.11	20.55	23.63	17.93	11.21	1.52	0.02
I_{opt}	312.51	639.87	2142.36	2775.17	2239.77	2278.58	2181.73
I_k	188.97	285.42	549.53	664.07	659.41	760.00	–

the situation that most resembles those encountered in tidal flats (Forster and Kromkamp, 2004; Jesus et al., 2006). In response to the surface incident light, fluorescence was produced from the surface down to the base of the photic layer of sediments (4 mm in our simulations, where tests were carried out down to 2 cm). As expected, because the received irradiance decreases with depth, the layer with the highest photosynthetic efficiency (α = 0.12; Table 6) was the surface layer (0–200 μm) and this parameter decreased with depth to zero at 4 mm. A dramatic decrease in this parameter occurred after a distance of 1 mm (α = 0.002) from the sediment surface. A significant increase in I_{opt} also occurred with increasing depth (Table 6). This parameter was minimal in the top surficial layer (312.51 μmol photons $m^{-2} s^{-1}$) and increased with depth, illustrating the progressive disappearance of photoinhibition that was observed only in the two top 200 μm sections, and to a lesser extent in the second layer. In deep layers (>0.6 mm), I_{opt} was higher than the maximum light tested (1200 μmol photons $m^{-2} s^{-1}$) and although all fitted curves were well adjusted ($R^2 > 0.98$), the parameter cannot be estimated accurately. The $rETR_{max}$ was also affected by the attenuation of light in the top layers and decreased with depth. An increase in I_k was also observed with increasing depth in response to the decrease in $rETR_{max}$ and α. In proportion to the light received at each position, the non-photochemical quenching (NPQ) followed the same tendency as the photosynthetic efficiency, with a gradual decrease from the upper layer to a depth of 4 mm, where the NPQ values reached minimum.

4. Discussion

Forster and Kromkamp (2004) stated that variable fluorescence measurements for quantifying rETR/I curves to estimate primary production rates in microphytobenthic biofilms from tidal flats are reliable when care is taken to consider the fine-scale of the depth distribution of microalgae. The fluorescence method is advantageous for estimating the rates of photosynthesis for intact biofilms in a vertical structure of natural sediment and because it provides an opportunity to multiply measurements to explore frequent temporal and spatial variability in response to environmental and biological dynamics. Perkins et al. (2011) reviewed the difficulties involved in interpreting fluorescence yields in biofilms in which the cells are capable of rapid and sometimes deep migratory rhythms (Frankenbach and Serôdio, 2017). Indeed, light has clearly been established as the main stimulus that microphytobenthic cells can handle through behavioral responses (migration) and physiological strategies involving NPQ induction (Mitbavkar and Anil, 2004; Perkins et al., 2011; Laviale et al., 2016). In this work, we focused on their dependence on light attenuation to decipher the factors responsible for changes in the light attenuation coefficient (k_d) and the implication of this coefficient for the estimation of photosynthetic parameters.

Our results confirm that the chl *a* profile that can differ in many ways at depth (homogeneous or established MPB biofilm, peak biomass production just below the surface, for instance) plays a key role in mitigating light attenuation with depth and therefore correction of the rETR/I curves. Indeed, we showed that, depending on the profile considered, uncorrected underestimation ranged between 19.09 and

53.11% for α, and between 12.23 and 39.11% on average for $rETR_{max}$, which is in line with Serôdio's (2004) claim and was also confirmed by Forster and Kromkamp (2004). The situation with maximum chl *a* in the subsurface layers (profile 2 in the present study) was the most subject to a high bias, while the lowest correction values were always recorded for a profile with an established MPB biofilm (profile 3 in the present study). A homogeneous profile always has intermediary values. In addition to reaffirming the importance of correcting the initially measured data, which was confirmed by our high minimum correction percentages, this work reinforces the importance of taking variations in chl *a* distribution with depth into account. Our results confirm the results of other works (Kühl and Jørgensen, 1992; Forster and Kromkamp, 2004; Serôdio, 2004; Forster et al., 2006; Jesus et al., 2006) demonstrating that measuring the vertical profile of chl *a* is essential because it is one of the main variables responsible for vertical stratification of primary production rates. Although the refined vertical profile may be difficult to measure in routine surveys, we recommend systematically coupling measurements of fluorescence data with the profile of chl *a* concentration in the photic layer, using, for instance, the "crème-brulée" technique (Laviale et al., 2015) or cryolanding techniques (De Brouwer and Stal, 2001; Kelly et al., 2001). The "crême brulée" technique was developed to measure the chl *a* concentration in the 0–200 μm layer. Combined with the value of 0–1 cm chl *a* concentration, it should be possible to imagine the shape of a chl *a* concentration profile, even if the vertical resolution is minimum in such case.

Apart from the importance of chlorophyll distribution in correcting fluorescence measurements – as already demonstrated - this work shows that it is also important to take the variability in sediment structure into account when estimating a light attenuation coefficient. Indeed, we have shown that, depending on the specific attenuation coefficient of the sediment particles ($k^{*}_{d(sed)} = 1\ mm^{-1}$ in sand and $4\ mm^{-1}$ in mud), without correction, underestimation of the same chl *a* profile can range from −1.25 to 3.42% for $rETR_{max}$ and from 13.90 to 20.05% for α. Thus, with the exception of the $rETR_{max}$ in a sandy environment with a homogeneous profile, the corrections were always higher in a muddy environment. These results confirm the significant role played by $k^{*}_{d(sed)}$ variability in light attenuation with depth and underline the error that can be made by using a constant value of this parameter in the calculation of k_d (Eq. (1)). Indeed, intertidal ecosystems are often characterized by heterogeneities and mixed sand and mud sediments (Orvain et al., 2012; Ubertini et al., 2012) and the variation in $k^{*}_{d(sed)}$ can rapidly change with a change in the sand-mud mixture (Kühl and Jørgensen, 1994). Even though the structure and the distribution of chlorophyll in the sediment with depth are hypothesized to be correlated (Jesus et al., 2006), the correction cannot be applied simply by evaluating the concentration of chl *a* in the upper layers and generalization should not only be based on the type of sediment. Sediment size should also be quantified and linked with $k^{*}_{d(sed)}$ to apply more robust corrections of light penetration and to avoid systematic underestimation, especially in muddy environments where the correction will be greater. The main objective of this paper is to propose an automatic correction tool for readers to apply rapid calculations on large data sets (see e-document in Excel; a Matlab version can be also provided on request).

The present results have several implications for the interpretation of microphytobenthic photosynthetic response to light variability. Beyond confirming that the photosynthetic parameters are underestimated (by up to 50% for α and 40% for $rETR_{max}$), our study underlines the role played by the nature of the sediment. In accordance with previous studies (Forster and Kromkamp, 2004), corrected rETR/I curves showed a true ecophysiological response with fewer photoinhibition mechanisms than apparent with raw fluorescence data. The decrease in rETR under high light may be due to fast-reversed down-regulation (xanthophyll cycle). Photosystem II regulations and xanthophyll cycle are the main physiological mechanisms involved in the photoprotection of epipelic benthic diatoms subjected to excessive saturating irradiance (Cartaxana et al., 2013). This study reveals that PAM measurements, when not corrected by light attenuation with depth, can cause artificial reduction of rETR at saturating light, which is generally interpreted as evidence for photoinhibition. Indeed, this reduction no longer appears after correction of the raw fluorescence data. This result reinforces the role played by migratory behavior by avoiding excessive light saturation and the remarkable adaptation fitness of these diatoms to the sediment matrix environment (Barnett et al., 2015). Physiological photoprotection is a complementary process that can be deployed by benthic diatoms to better withstand high light levels. Migration, is however, the most efficient process and probably the best strategy to avoid excessive energy costs such as activation of the xanthophyll cycle. Cartaxana et al. (2011) showed the prevalence of the use of migration of epipelic diatoms inhabiting muddy sediments to protect themselves against high light, while only physiological protection strategies were observed in sandy sediments. Our study emphasizes differences in light penetration between mud and sand and shows that the proposed correction can be used to readjust the photosynthetic parameters in both environments because distortion was observed, whatever the granulometry.

Our study improves the applicability of fundamental scientific findings made in recent decades for accurate accounting of irradiance. This is particularly true when the role of light in photobiological processes in sediments is being investigated. The correction proposed in this study as a function of chl *a* depth profiling and granulometry takes the most relevant factors affecting light penetration into account, but further refinement of the model is possible for future studies. For instance, Perkins et al. (2011) reported that PAM is intrusive in terms of rapidly exposing cells to darkness in the first few minutes by exposing cells to drastic exposure to irradiance, which could artificially trigger migration due to photoinhibition or photo-kinesis. Frankenbach and Serôdio (2017) used a PAM fluorescence survey to demonstrate the chronobiological migration of MPB and the impact on photosynthetic parameters. The measurement of F_0 (fluorescence in darkness) could thus be surveyed in parallel to better detect the potential artificial migration provoked by exposure to darkness. Similarly, since biofilms are very motile and patchy, a subsample core taken in nearby area might not be sufficiently precise for chl *a* profiling across depths in the actual area sampled with PAM. We recommend taking samples very close to the experimental area with the PAM. Estimating the attenuation of light caused by sediment composition could also be improved by measurements of light attenuation in a range of sand-mud mixture and various mineralogical compositions. Similarly, the distance crossed by the photons in air can be affected by a specific attenuation before reaching the sediment surface. This is very important as the distance between the optic fiber and the air-sediment interface must be controlled, but also the angle of actinic light at the sediment surface which is able of interact (Perkins et al., 2011). This specific issue could contribute to the difficulties involved in using the imaging-PAM fluorometer, since 3D micro-topography can modify the 3D field of distances crossed by photons in the air. Further numerical equations could thus be developed and added to the correction tool to account for the light attenuation in the air, if micro-topography is measured in parallel. The role of chl *a* depth profiling is the main process controlling the light attenuation in the sediment euphotic layer. However, the presence of breakdown products (e.g. photo-oxidized chl *a* after grazing by deposit-feeders) can also lead to accumulation of phaeopigments that may be also involved in k_d changes. Depending on the composition of the multi-species assemblage of the biofilm, the presence of accessory pigments (carotenoids, phycobiliproteins) could also be taken into account by using a field spectro-radiometer sensor or extraction of the pigments, then analyzed with HPLC (Jesus et al., 2006). Even if these substances are generally considered as transparent (Decho, 1990), the amount of EPS produced by diatoms during MPB migration could also induce specific light attenuation. All these factors could affect the estimation of k_d before correction.

Acknowledgements

We are grateful to GIP Seine-Aval for funding the two related programs (Seine-Aval 5) BARBES and PROUESSE. This work also benefited from fruitful discussions with Sébastien Lefebvre. We would like to sincerely thank the 3 anonymous referees for their comments and contribution.

Appendix A. Supplementary data

Supplementary data to this article can be found online at https://doi.org/10.1016/j.jembe.2018.02.007.

References

Aberle-Malzahn, N., 2004. The Microphytobenthos and its Role in Aquatic Food Webs. Universität Kiel.
Admiraal, W., 1984. The ecology of estuarine sediment-inhabiting diatoms. In: Progress in Phycological Research, pp. 269–322.
Admiraal, W., Beukema, J., Van Es, F.B., 1985. Seasonal fluctuations in the biomass and metabolic activity of bacterioplankton and phytoplankton in a well-mixed estuary: the Ems-Dollard (Wadden Sea). J. Plankton Res. 7, 877–890.
Baillie, P.W., Welsh, B.L., 1980. The effect of tidal resuspension on the distribution of intertidal epipelic algae in an estuary. Estuar. Coast. Mar. Sci. 10, 165–180.
Barnett, A., Méléder, V., Blommaert, L., Lepetit, B., Gaudin, P., Vyverman, W., Sabbe, K., Dupuy, C., Lavaud, J., 2015. Growth form defines physiological photoprotective capacity in intertidal benthic diatoms. ISME J. 9, 32–45.
Barranguet, C., Kromkamp, J., 2000. Estimating primary production rates from photosynthetic electron transport in estuarine microphytobenthos. Mar. Ecol. Prog. Ser. 204, 39–52.
Benyoucef, I., Blandin, E., Lerouxel, A., Jesus, B., Rosa, P., Méléder, V., Launeau, P., Barillé, L., 2014. Microphytobenthos interannual variations in a north-European estuary (Loire estuary, France) detected by visible-infrared multispectral remote sensing. Estuar. Coast. Shelf Sci. 136, 43–52.
Blanchard, G.F., Guarini, J.-M., Richard, P., Gros, P., Mornet, F., 1996. Quantifying the short-term temperature effect on light-saturated photosynthesis of intertidal mircophytobenthos. Mar. Ecol. Prog. Ser. 134, 309–313.
Blanchard, G.F., Guarini, J.-M., Orvain, F., Sauriau, P.-G., 2001. Dynamic behaviour of benthic microalgal biomass in intertidal mudflats. J. Exp. Mar. Biol. Ecol. 264, 85–100.
Cartaxana, P., Ruivo, M., Hubas, C., Davidson, I., Serôdio, J., Jesus, B., 2011. Physiological versus behavioral photoprotection in intertidal epipelic and epipsammic benthic diatom communities. J. Exp. Mar. Biol. Ecol. 405, 120–127.
Cartaxana, P., Domingues, N., Cruz, S., Jesus, B., Laviale, M., Serôdio, J., Da Silva, J.M., 2013. Photoinhibition in benthic diatom assemblages under light stress. Aquat. Microb. Ecol. 70, 87–92.
Chukhutsina, V.U., Büchel, C., van Amerongen, H., 2014. Disentangling two non-photochemical quenching processes in *Cyclotella meneghiniana* by spectrally-resolved picosecond fluorescence at 77 K. Biochim. Biophys. Acta 1837, 899–907.
Cloern, J.E., Foster, S.Q., Kleckner, a.E., 2014. Phytoplankton primary production in the world's estuarine-coastal ecosystems. Biogeosciences 11, 2477–2501.
De Brouwer, J.F.C., Stal, L.J., 2001. Short-term dynamics in microphytobenthos distribution and associated extracellular carbohydrates in surface sediments of an intertidal mudflat. Mar. Ecol. Prog. Ser. 218, 33–44.
De Jonge, V.N., Van Beuselom, J.E.E., 1992. Contribution of resuspended microphytobenthos to total phytoplankton in the EMS estuary and its possible role for grazers. Neth. J. Sea Res. 30, 91–105.
Decho, A.W., 1990. Microbial exopolymer secretions in ocean environments: their role(s) in food webs and marine processes. Oceanogr. Mar. Annu. Rev. 28, 73–153.
Decho, A.W., 2000. Microbial biofilms in intertidal systems: an overview. Cont. Shelf Res. 20, 1257–1273.
Dupuy, C., Mallet, C., Guizien, K., Montanié, H., Bréret, M., Mornet, F., Fontaine, C., Nérot, C., Orvain, F., 2014. Sequential resuspension of biofilm components (viruses, prokaryotes and protists) as measured by erodimetry experiments in the Brouage mudflat (French Atlantic coast). J. Sea Res. 92, 56–65.
Edgar, L.A., Pickett-Heaps, J.D., 1984. Valve morphogenesis in the pennate diatom Navicula cuspidata. J. Phycol. 20, 47–61.
Eilers, P.H.C., Peeters, J.C.H., 1988. A model for the relationship between light intensity and the rate of photosynthesis in phytoplankton. Ecol. Model. 42, 199–215.
Fagherazzi, S., Mariotti, G., Banks, A.T., Morgan, E.J., Fulweiler, R.W., 2014. The relationships among hydrodynamics, sediment distribution, and chlorophyll in a mesotidal estuary. Estuar. Coast. Shelf Sci. 144, 54–64.
Forster, R.M., Kromkamp, J.C., 2004. Modelling the effects of chlorophyll fluorescence from subsurface layers on photosynthetic efficiency measurements in microphytobenthic algae. Mar. Ecol. Prog. Ser. 284, 9–22.
Forster, R.M., Créach, V., Sabbe, K., Vyverman, W., Stal, L.J., 2006. Biodiversity-ecosystem function relationship in microphytobenthic diatoms of the Westerschelde estuary. Mar. Ecol. Prog. Ser. 311, 191–201.
Frankenbach, S., Serôdio, J., 2017. One pulse, one light curve: fast characterization of the light response of microphytobenthos biofilms using chlorophyll fluorescence. Limnol. Oceanogr. Methods 15, 554–566.
Geider, R.J., Delucia, E.H., Falkowski, P.G., Finzi, A.C., Grime, J.P., Grace, J., Kana, T.M., Roche, J.L.A., Long, S.P., Osborne, B.A., Platt, T., Prentice, I.C., Raven, J.A., Schlesinger, W.H., Smetacek, V., Stuart, V., Box, P.O., 2001. Primary Productivity of Planet Earth: Biological Determinants and Physical Constraints in Terrestrial and Aquatic Habitats.
Guarini, J.-M., Blanchard, G.F., Gros, P., 2000. Quantification of the microphytobenthic primary production in European intertidal mudflats – a modelling approach. Cont. Shelf Res. 20, 1771–1788.
Hartig, P., Wolfstein, K., Lippemeier, S., Colijn, F., 1998. Photosynthetic activity of natural microphytobenthos populations measured by fluorescence (PAM) and ^{14}C-tracer methods: a comparison. Mar. Ecol. Prog. Ser. 166, 53–62.
Herman, P.M.J., Middelburg, J.J., Widdows, J., Lucas, C.H., Heip, C.H.R., 2000. Stable isotopes as trophic tracers: combining field\sampling and manipulative labelling of food\resources for macrobenthos. Mar. Ecol. Prog. Ser. 204, 79–92.
Jesus, B., Brotas, V., Marani, M., Paterson, D.M., 2005. Spatial dynamics of microphytobenthos determined by PAM fluorescence. Estuar. Coast. Shelf Sci. 65, 30–42.
Jesus, B., Mendes, C.R., Brotas, V., Paterson, D.M., 2006. Effect of sediment type on microphytobenthos vertical distribution: modelling the productive biomass and improving ground truth measurements. J. Exp. Mar. Biol. Ecol. 332, 60–74.
Johnsen, G., Sakshaug, E., 2007. Biooptical characteristics of PSII and PSI in 33 species (13 pigment groups) of marine phytoplankton, and the relevance for pulse-amplitude-modulated and fast-repetition-rate fluorometry 1. J. Phycol. 43, 1236–1251.
Juneau, P., Barnett, A., Méléder, V., Dupuy, C., Lavaud, J., 2015. Combined effect of high light and high salinity on the regulation of photosynthesis in three diatom species belonging to the main growth forms of intertidal flat inhabiting microphytobenthos. J. Exp. Mar. Biol. Ecol. 463, 95–104.
Kang, C.-K., Park, H.J., Choy, E.J., Choi, K.-S., Hwang, K., Kim, J., 2015. Linking intertidal and subtidal food webs: consumer-mediated transport of intertidal benthic microalgal carbon. PLoS One 10 (10), e0139802. http://dx.doi.org/10.1371/journal.pone.0139802.
Kelly, J.A., Honeywill, C., Paterson, D.M., 2001. Microscale analysis of chlorophyll-a in cohesive, intertidal sediments: the implications of microphytobenthos distribution. J. Mar. Biol. Assoc. UK 81, 151–162.
Kirk, J., 1983. Light and Photosynthesis in Aquatic Ecosystems. Cambridge University Press, Cambridge.
Kromkamp, J., Barranguet, C., Peene, J., 1998. Determination of microphytobenthos PSII quantum efficiency and photosynthetic activity by means of variable chlorophyll fluorescence. Mar. Ecol. Prog. Ser. 162, 45–55.
Kühl, M., Jørgensen, B.B., 1992. Spectral light measurements in microbenthic phototrophic communities with a fiber-optic microprobe coupled to a sensitive diode array detector. Limonol. Oceanogr. 37, 1813–1823.
Kühl, M., Jørgensen, B.B., 1994. The light-field of microbenthic communities- radiance distribution and microscale optics of sandy coastal sediments. Limnol. Oceanogr. 39, 1368–1398.
Kühl, M., Lassen, C., Jørgensen, B.B., 1994. Light penetration and light intensity in sandy marine sediments measured with irradiance and scalar irradiance fiber-optic microprobes. Mar. Ecol. Prog. Ser. 105, 139–148.
Laviale, M., Ezequiel, J., Pais, C., Cartaxana, P., Serôdio, J., 2015. The “crème brûlée” sampler: a new high-resolution method for the fast vertical sampling of intertidal fine sediments. J. Exp. Mar. Biol. Ecol. 468, 37–44.
Laviale, M., Frankenbach, S., Serôdio, J., 2016. The importance of being fast: comparative kinetics of vertical migration and non-photochemical quenching of benthic diatoms under light stress. Mar. Biol. 163, 1–12.
Lubarsky, H.V., Hubas, C., Chocholek, M., Larson, F., Manz, W., Paterson, D.M., Gerbersdorf, S.U., 2010. The stabilisation potential of individual and mixed assemblages of natural bacteria and microalgae. PLoS One 5, e13794.
Lucas, C.H., Holligan, P.M., 1999. Nature and ecological implications of algal pigment diversity on the Molenplaat tidal flat (Westerschelde estuary, SW Netherlands). Mar. Ecol. Prog. Ser. 180, 51–64.
Middelburg, J.J., Barranguet, C., Boschker, H.T.S., Herman, P.M.J., Moens, T., Heip, C.H.R., 2000. The fate of intertidal microphytobenthos carbon: an in situ ^{13}C-labeling study. Limnol. Oceanogr. 45, 1224–1234.
Mitbavkar, S., Anil, a.C., 2004. Vertical migratory rhythms of benthic diatoms in a tropical intertidal sand flat: influence of irradiance and tides. Mar. Biol. 145, 9–20.
Morris, E.P., Kromkamp, J.C., 2003. Influence of temperature on the relationship between oxygen- and fluorescence-based estimates of photosynthetic parameters in a marine benthic diatom (*Cylindrotheca closterium*). Eur. J. Phycol. 38, 133–142.
Orvain, F., Galois, R., Barnard, C., Sylvestre, A., Blanchard, G., Sauriau, P.-G., 2003. Carbohydrate production in relation to microphytobenthic biofilm development: an integrated approach in a tidal mesocosm. Microb. Ecol. 45, 237–251.
Orvain, F., Lefebvre, S., Montepini, J., Sébire, M., Gangnery, A., Sylvand, B., 2012. Spatial and temporal interaction between sediment and microphytobenthos in a temperate estuarine macro-intertidal bay. Mar. Ecol. Prog. Ser. 458, 53–68.
Perkins, R.G., Underwood, G.J.C., Brotas, V., Snow, G.C., Jesus, B., Ribeiro, L., 2001. Responses of microphytobenthos to light: primary production and carbohydrate allocation over an emersion period. Mar. Ecol. Prog. Ser. 223, 101–112.
Perkins, R.G., Honeywill, C., Consalvey, M., Austin, H.A., Tolhurst, T.J., Paterson, D.M., 2003. Changes in microphytobenthic chlorophyll a and EPS resulting from sediment compaction due to de-watering: opposing patterns in concentration and content. Cont. Shelf Res. 23, 575–586.
Perkins, R.G., Kromkamp, J.C., Serôdio, J., Lavaud, J., Jesus, B., Mouget, J.-L., Lefebvre, S., Forster, R.M., 2011. The application of variable chlorophyll fluorescence to microphytobenthic biofilms. In: Chlorophyll a Fluorescence in Aquatic Sciences: Methods and Applications.
Pinckney, J., Zingmark, R., 1991. Effects of tidal stage and sun angles on intertidal benthic microalgal productivity. Mar. Ecol. Prog. Ser. 76, 81–89.

Ploug, H., Lassen, C., Järgensen, B.B., 1993. Action spectra of microalgal photosynthesis and depth distribution of spectral scalar irradiance in a coastal marine sediment of Limfjorden, Denmark. FEMS Microbiol. Ecol. 11, 261–270.
Schreiber, U., Klughammer, C., Kolbowski, J., 2012. Assessment of wavelength-dependent parameters of photosynthetic electron transport with a new type of multi-color PAM chlorophyll fluorometer. Photosynth. Res. 113, 127–144.
Serôdio, J., 2003. A chlorophyll fluorescence index to estimate short-term rates of photosynthesis by intertidal microphytobenthos. J. Phycol. 39, 33–46.
Serôdio, J., 2004. Analysis of variable chlorophyll fluorescence in microphytobenthos assemblages: implications of the use of depth-integrated measurements. Aquat. Microb. Ecol. 36, 137–152.
Serôdio, J., Catarino, F., 2000. Modelling the primary productivity of intertidal microphytobenthos: time scales of variability and effects of migratory rhythms. Mar. Ecol. Prog. Ser. 192, 13–30.
Serôdio, J., Lavaud, J., 2011. A model for describing the light response of the non-photochemical quenching of chlorophyll fluorescence. Photosynth. Res. 108, 61–76.
Serôdio, J., Da Silva, J.M., Catarino, F., 1997. Nondestrusive tracing of migratory rhytms of intertidal benthic microalgea using in vivo chlorophyll a fluorescence. J. Phycol. 33, 542–553.
Serôdio, J., Vieira, S., Barroso, F., 2007. Relationship of variable chlorophyll fluorescence indices to photosynthetic rates in microphytobenthos. Aquat. Microb. Ecol. 49, 71–85.
Serôdio, J., Ezequiel, J., Barnett, A., Mouget, J.L., Meĺéder, V., Laviale, M., Lavaud, J., 2012. Efficiency of photoprotection in microphytobenthos: role of vertical migration and the xanthophyll cycle against photoinhibition. Aquat. Microb. Ecol. 67, 161–175.
Sutherland, T.F., Grant, J., Amos, C.L., 1998. The effect of carbohydrate production by the diatom *Nitzschia curvilineata* on the erodibility of sediment. Limnol. Oceanogr. 43, 65–72.
Taylor, W.R., 1964. Light and photosynthesis in intertidal benthic diatoms. Helgoländer Meeresun. 10, 29–37.
Thrush, S.F., Hewitt, J.E., Lohrer, A.M., Chiaroni, L.D., 2013. When small changes matter: the role of cross-scale interactions between habitat and ecological connectivity in recovery. Ecol. Appl. 23, 226–238.
Tolhurst, T.J., Jesus, B., Brotas, V., Paterson, D.M., 2003. Diatom migration and sediment armouring - an example from the Tagus Estuary, Portugal. Hydrobiologia 503, 183–193.
Tolhurst, T.J., Defew, E.C., De Brouwer, J.F.C., Wolfstein, K., Stal, L.J., Paterson, D.M., 2006. Small-scale temporal and spatial variability in the erosion threshold and properties of cohesive intertidal sediments. Cont. Shelf Res. 26, 351–362.
Ubertini, M., Lefebvre, S., Gangnery, A., Grangeré, K., Le Gendre, R., Orvain, F., 2012. Spatial variability of benthic-pelagic coupling in an estuary ecosystem: consequences for microphytobenthos resuspension phenomenon. PLoS One 7, e44155.
Underwood, G.J.C., Kromkamp, J., 1999. Primary production by phytoplankton and microphytobenthos in estuaries. Adv. Ecol. Res. 29, 93–153.
Underwood, G.J.C., Smith, D.J., 1998. Predicting epipelic diatom exopolymer concentrations in intertidal sediments from sediment chlorophyll a. Microb. Ecol. 35, 116–125.
Van Kooten, O., Snel, J.F.H., 1990. The use of chlorophyll fluoresence nomenclature in plant stress physiology. Photosynth. Res. 25, 147–150.
Vieira, S., Ribeiro, L., Jesus, B., Cartaxana, P., Da Silva, J.M., 2013. Photosynthesis assessment in microphytobenthos using conventional and imaging pulse amplitude modulation fluorometry. Photochem. Photobiol. 89, 97–102.
Webb, W.L., Newton, M., Starr, D., 1974. Carbon dioxide exchange of *Alnus rubra*. Oecologia 17, 281–291.
Weerman, E.J., Herman, P.M.J., Van De Koppel, J., 2011. Macrobenthos abundance and distribution on a spatially patterned intertidal flat. Mar. Ecol. Prog. Ser. 440, 95–103.